Applied Materials Today 24 (2021) 101139

Contents lists available at ScienceDirect

Applied Materials Today

journal homepage: www.elsevier.com/locate/apmt

# Stacked carbon paper electrodes with pseudo-channel effect to improve flow characteristics of electrolyte in vanadium redox flow batteries

Jae-Moon Jeong[a], Kwang Il Jeong[a], Jae Hyung Oh[a], Yong Sik Chung[b], Seong Su Kim[a,*]

[a] Department of Mechanical Engineering, Korea Advanced Institute of Science and Technology (KAIST), 291, Dahak-ro, Yuseong-gu, Daejeon 305-701, Republic of Korea

[b] Department of Organic Materials and Fiber Engineering, Chonbuk National University, 567 Baekje-daero, Deokjin-gu, Jeonju-si, Jeollabuk-do, Republic of Korea

ARTICLE INFO

*Article history:*
Received 24 May 2021
Revised 14 July 2021
Accepted 26 July 2021

*Keywords:*
Vanadium redox flow battery
Electrode
Carbon paper (CP)
Holey pattern
Pseudo-channel effect

ABSTRACT

Recently, carbon papers (CPs) have attracted much attention as alternative electrode materials for vanadium redox flow batteries (VRFBs) because of large redox reaction sites owing to their high fiber volume fraction compared with the conventional electrode material, carbon felts (CFs). However, the low permeability of CPs in the in-plane direction tends to cause the side flow of electrolytes around the electrode, which in turn leads to an uneven flow of electrolytes. Therefore, until now, CPs have been applied only to flow-by type VRFBs. In this study, a method is developed to enhance the performance of CP electrodes with a pseudo-channel effect by means of holey patterns of the CP to apply flow-through type VRFBs. The electrolyte flow characteristics and electrochemical properties are analyzed through numerical simulations and cyclic voltammetry tests, respectively. The performances of the electrodes are analyzed through VRFB single-cell tests. As a result of numerical analysis, it is confirmed that the overall flow rate inside the electrode increases substantially, and the flow distribution becomes uniform owing to the pseudo-channel effect, which leads to an increase in efficiency. At a current density of 100 mA $cm^{-2}$, the energy efficiency of the H-CP electrode (85.11%) increases by 10.41% and 4.34%, compared with the corresponding values of unpatterned CP and heat-treated CF electrodes, respectively.



## 1. Introduction

Renewable energy resources and technologies have attracted much attention for their ability to provide a large number of environmental benefits by reducing emissions from fossil fuels. However, renewable energy sources depend highly on the location and natural environment, causing the production to be unstable, which is a significant problem. For the stable supply of renewable energy, an energy storage system (ESS) is one of the solutions to compensate for inconsistent production and meet the steady power demand. Vanadium redox flow batteries (VRFBs), one of the representative ESSs, have the advantage of design flexibility in power and capacity and high durability over 30 years [1–12]. Besides, VRFBs are attracting attention as next-generation ESSs because they have the benefit of safety from explosion and fire. However, the low energy efficiency (EE) of VRFBs must be improved to expand their applications.

In VRFBs, the electrochemical potential difference is induced by a redox reaction of the electrolyte at the active sites of the electrode. Therefore, the electrochemical property of the electrode greatly affects the EE of the VRFB. Carbon felt (CF) has been widely used as an electrode material owing to its high permeability, high electrical conductivity, and chemical stability against strong acids [13–16]. However, CFs have inert surface activities of the pristine materials and small redox reaction sites owing to their low fiber volume fraction of less than 8%, which results in poor electrochemical properties. To increase the EE of the entire system, many studies have been conducted to improve the electrochemical properties of CFs using various methods, such as metallization and electrodeposition [17–21]. However, the inherent low fiber volume fractions of the CFs, the complexity of the process, and the increased manufacturing cost act as limitations in solving the problem. Therefore,

* Corresponding author.
*E-mail address:* seongsukim@kaist.ac.kr (S.S. Kim).

https://doi.org/10.1016/j.apmt.2021.101139

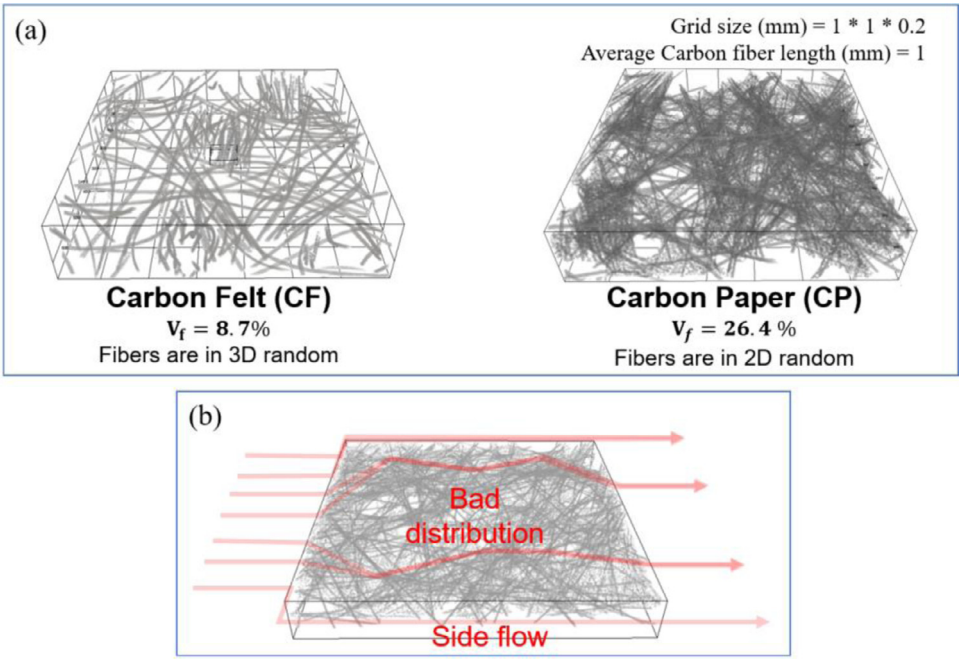


**Fig. 1.** Comparison of carbon felts and carbon papers; (a) Micro-CT images, (b) Flow field inside of a carbon paper.

to improve the EE of VRFBs, it is necessary to replace the CF with one that has a high fiber volume fraction.

Several alternative materials for CFs have been proposed [22–24]. Among them, there have been studies using carbon papers (CPs) that have relatively high electrochemical properties due to the high fiber volume fraction ($v_f > 20\%$), as shown in Fig. 1(a) [25–32]. A typical VRFB stack undergoes a redox reaction as the electrolyte flows through the electrode (Flow-through model) with a thin bipolar plate. For CP electrodes, however, the low porosity and random fiber arrangement in the in-plane direction tend to cause side flow of the electrolyte around the electrode, which leads to an uneven electrolyte flow, as shown in Fig. 1(b) [33]. Therefore, previous studies using CP electrodes focused on the "flow-by model" as a way to improve the utilization of the reaction site by processing channels on a bipolar plate as shown in Fig. S1. In the “flow-by model”, however, most electrolytes flow through the channels on the bipolar plates, which has low flow rate through the electrode. To increase the utilization of the electrodes in the thickness direction, the flow channel design was changed, and the perforations were machined in the CPs along the channel of the bipolar plate [28–32]. However, these methods not only increase the system size and manufacturing cost of the bipolar plate but also show inherent pressure drop issues that reduce overall system efficiency, requiring more consideration for practical applications [34]. Furthermore, the flow in the in-plane direction of the electrodes, which can dramatically improve the reaction site, may not be greatly increased. In particular, when a number of holes are drilled in the CP to induce the flow in the thickness direction, the electrical conductivity and reaction sites are greatly reduced due to the substantial loss of the electrode volume which limits the efficiency improvement [28,29].

In this study, a method to induce uniform electrolyte distribution by patterning on the CPs at uniform intervals without any machining process of the bipolar plates was developed to apply flow-through type VRFBs. An electrode sample was prepared using a laser by stacking 20 layers of CP that had a laser-punched holey pattern in the thickness direction. The electrolyte flow characteristics and electrochemical properties with respect to the patterns were analyzed by means of numerical simulations and cyclic voltammetry (CV) tests, respectively. Subsequently, a VRFB single-cell test was conducted to evaluate the electrode performance according to the pattern shape.

## 2. Experimental and computational procedures

### 2.1. Preparation of the patterned electrodes

CP electrodes were prepared with three types of pattern as shown in Fig. 2(a). In the case of the laser-punched holey CP (H-CP), 100 holes were fabricated for each ply. The spacing between the holes was kept constant at 3 mm, but three kinds of hole size were used: 0.4, 0.5, and 0.6 mm. The V-grooved CP (V-CP), which provides flow channels in the flow direction, was prepared for comparison with the H-CP. The V-shaped grooves were uniformly distributed over the entire electrode, and the width and interval of the grooves were 0.1 and 1 mm, respectively.

Details of the fabrication procedure of the CP electrodes are shown in Fig. 2(b). A laser cutting machine (L4060, REXBOT, Republic of Korea) was used to cut a CP (JNT 20, JNTG, Republic of Korea) with a thickness of 200 $\mu$m into a size of 30 $\times$ 30 mm, and the patterns were formed on the CPs thereafter. The output power and cutting speed of the laser cutting machine were set to 80 W and 10 mm $s^{-1}$, respectively. After laser processing, the CPs were washed in distilled water for 1 min using ultrasonic waves (POWERSONIC 610, KLEENTEK, Korea) to remove the residue generated on the edge and around the holes of the electrode. Subsequently, the CPs were dried at 80 °C for 30 min, and 20 plies of CPs were stacked in the cell stack to make a 4-mm-thick electrode. In addition, a CF electrode made with heat-treated carbon felt (XF30A, TOYOBO, JAPAN), which is generally used for VRFB electrodes, was prepared with the same dimensions to compare the efficiency.

### 2.2. Measurement of areal specific resistance

The areal specific resistance (ASR) of the electrode can affect the ohmic loss during the VRFB performance test, which is associated with the voltage efficiency during the VRFB cell test. The ASR of each electrode was measured using an LCR meter (E4980A,

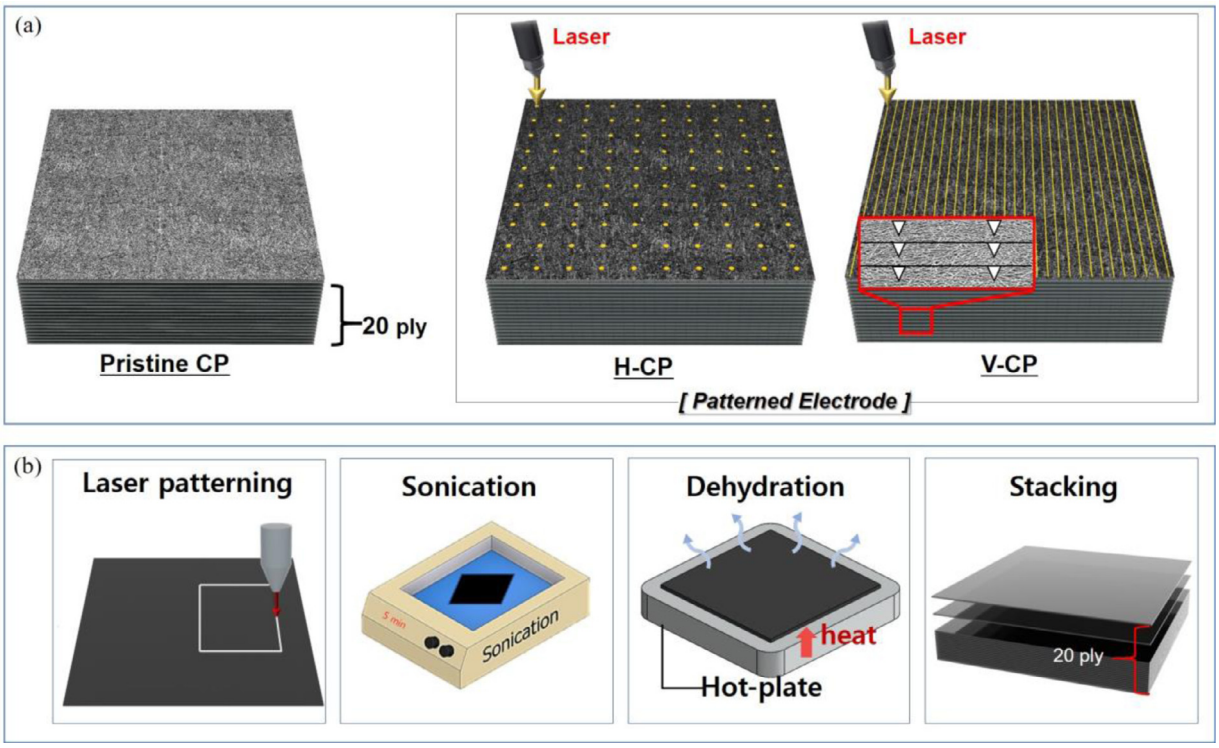


**Fig. 2.** Patterns of the carbon papers (CP); (a) Schematic diagram of the CP, (b) preparation process of CP electrodes.

Keysight, USA) connected to a copper plate. The CP electrodes machined to a size of 30 × 30 mm were placed between gold-coated copper plates, after which the electrical resistance was measured at 25% compression using a universal testing machine (INSTRON 4469, Instron Corp, MA, USA).

### 2.3. Measurements of electrochemical performances

CV tests were performed to measure the electrochemical properties of the specimens using a potentiometer (WBSC3000M2, WonA Tech, Republic of Korea). A CP specimen, platinum gauge electrode, and standard calomel electrode (SCE) were used as the working, counter, and reference electrodes, respectively. As electrolytes, 0.1-M $VO^{2+}$ and 2-M $H_2SO_4$ solutions were used. To evaluate the electrochemical properties of the positive redox couple ($VO^{2+}/VO_2^{+}$), the potential range and scan rate were set to 0–1.5 V (versus SCE) and 5 $mVs^{-1}$, respectively.

### 2.4. Numerical analysis to characterize the electrolyte flow

The electrolyte flow characteristics with respect to the pattern of the CPs were analyzed by means of numerical simulations using the commercial tool FLUENT (ANSYS FLUENT 2020 R1, Ansys Inc., USA). As shown in Fig. 3, the electrode and flow frame shapes were created using DesignModeler (ANSYS DesignModeler 2020 R1, Ansys Inc., USA) in ANSYS Workbench (ANSYS Workbench 2020 R1, Ansys Inc., USA) and meshed to generate the finite elements by using Meshing (ANSYS Meshing, Ansys Inc., USA).

As the boundary conditions, the flow rate of the electrolyte at the inlet was set to 80 mL/min, and the atmospheric pressure condition was applied to the outlet. The flow was assumed to be laminar. The properties of the electrode and electrolyte are summarized in Table 1 [35,36].

**Table 1**
Material properties for numerical simulation.

| | | |
|---|---|---|
| Material properties of electrolyte [35] | | |
| Density | $kg/m^3$ | 1350 |
| Viscosity | kg/(m•s) | $4.93 \times 10^{-3}$ |
| Material properties of carbon paper [36] | | |
| Permeability (In-plane) | $m^2$ | $1.44 \times 10^{-11}$ |
| Permeability (Out of plane) | $m^2$ | $9.17 \times 10^{-12}$ |

### 2.5. VRFB single-cell tests

A schematic diagram of the cell test bench is shown in Fig. S2. The VRFB single-cell consisted of end plates, current collectors, bipolar plates, gaskets, flow frames, electrodes with the active area of 9.0 $cm^2$, and membranes (NAFION 212, EI DuPont, USA). The electrolyte of 1.7-M $VOSO_4$ and 4.2-M $H_2SO_4$ aqueous solution was circulated at a rate of 80 mL/min, and nitrogen gas was purged in the electrolyte tank before the cell test to prevent oxidation of vanadium. A charge–discharge test was performed for 30 cycles at a constant current density of 100 mA $cm^{-2}$, and the cutoff voltage was set to 1.6 V for charging and 1.0 V for discharging.

## 3. Results and discussion

### 3.1. Surface morphologies of the CPs

Optical microscope (OM) images of the prepared CPs are shown in Fig. 4. As shown in Fig. 4(a), the surface of the pristine CP had a dense structure without large cavities owing to the random arrangement of carbon fibers and the presence of the binder, which led to poor electrolyte flow. To increase the reactive surface area of the electrode by inducing a uniform flow, a flow path was created on the pristine CP, as shown in Fig. 4(b,c). Fig. 4(b) shows the OM images of the H-CP with respect to the hole sizes. It was confirmed that the average diameters of the hole were 396.8 ± 10.4,

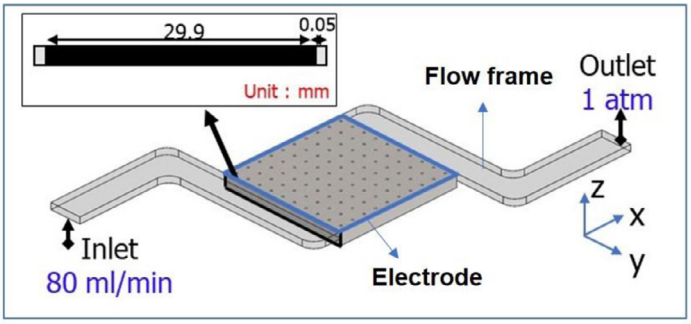


(a)

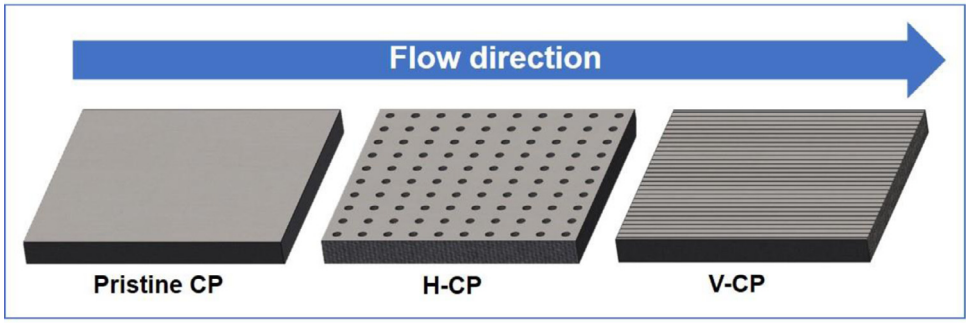


(b)

**Fig. 3.** Flow frame and electrode for numerical simulation; (a) geometry for numerical simulation, (b) schematic diagram of the stacked CP electrode.

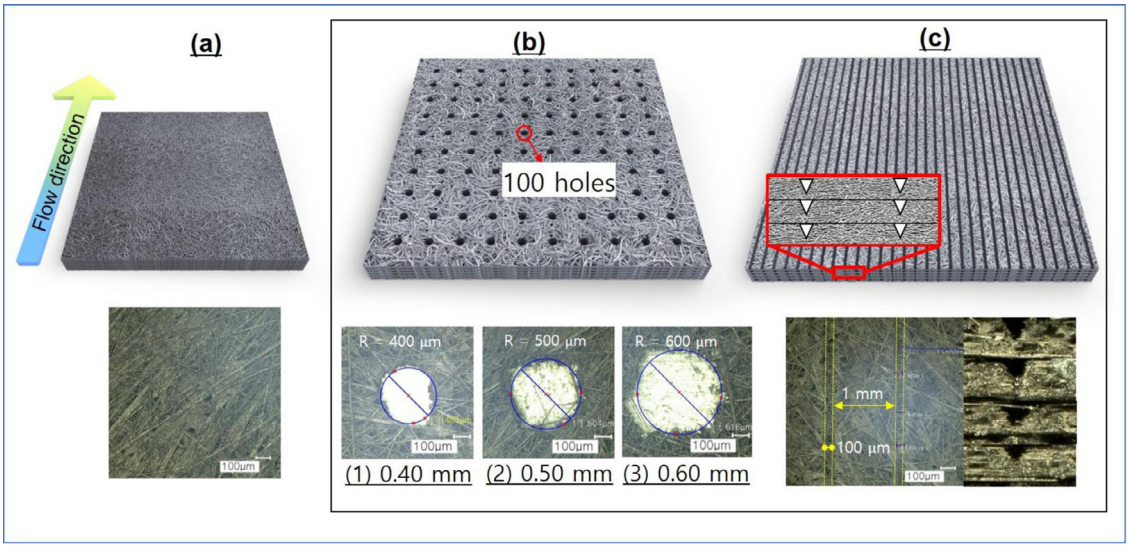


**Fig. 4.** Optical microscope (OM) images of the stacked CP electrode; (a) Pristine CP, (b) H-CP, (c) V-CP.

502.6 ± 15.4, and 603.5 ± 13.6 $\mu$m, as intended, and the fiber arrangement of the remaining parts did not change after laser cutting when compared with the pristine CP. The V-CP shown in Fig. 4(c) was machined with a groove width of 105.3 ± 12.3 $\mu$m and an interval of 1002 ± 33.1 $\mu$m.

### 3.2. Electrical conductivity and electrochemical properties

Table 2 shows the ASR and apparent volume of the stacked CP electrodes. The apparent volume was calculated to check the volume reduction by machining the holey patterns and grooves. Compared with the pristine CP electrode, the two patterned electrodes showed a volume decrease of 2%, resulting in a reduced apparent reaction volume with the electrolyte. The reduced volume caused increased ASR because the electrical path was partially eliminated by the patterns as shown in Fig. S3. The ASR of the CF electrode was lower than those of the CP electrodes because most fibers of

**Table 2**
Areal surface resistance and apparent volume of the stacked CP electrodes.

| Name | ASR(mΩ cm$^2$) | Apparent volume(mm$^3$) |
|---|---|---|
| H-CP ($d$ = 0.6 mm) | 170.5 (−70.3%) | 2615 (−3.1%) |
| H-CP ($d$ = 0.5 mm) | 135.8 (−35.7%) | 2641 (−2.2%) |
| H-CP ($d$ = 0.4 mm) | 118.6 (−18.5%) | 2662 (−1.4%) |
| V-CP | 135.0 (−34.9%) | 2634 (−2.1%) |
| Pristine CP | 100.1 | 2700 |
| Heat treated CF | 88.9 | 2700 |
| | | (% of Pristine CP) |

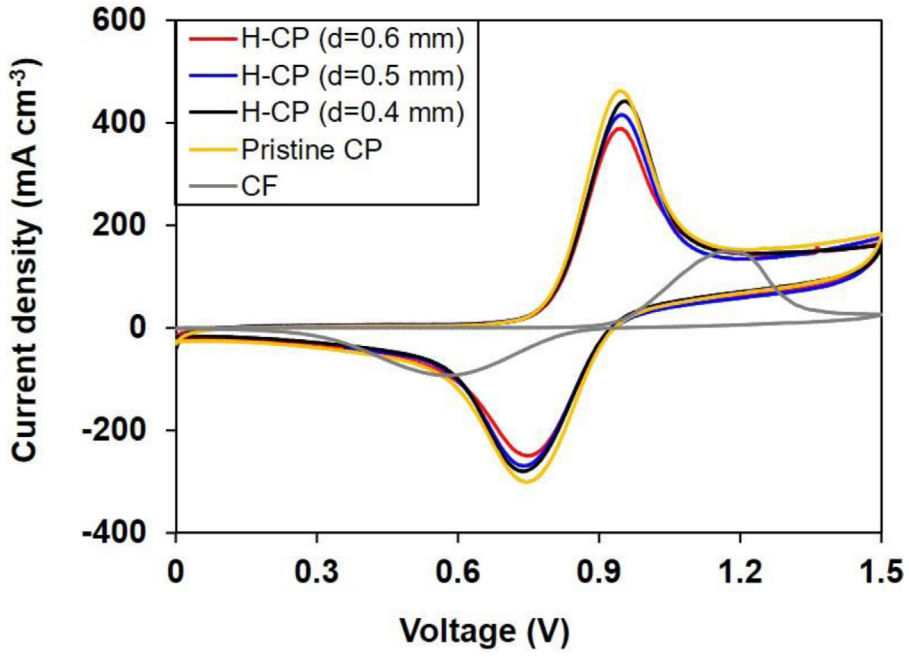


**Fig. 5.** CV curves of electrodes.

**Table 3**
Electrochemical properties of the stacked CP electrodes.

| Name | $I_{pa}$ (mA/cm$^3$) | $I_{pc}$ (mA/cm$^3$) | $\Delta E$ (V) |
|---|---|---|---|
| H-CP ($d$ = 0.6 mm) | 382.03 | 244.31 | 0.20 |
| H-CP ($d$ = 0.5 mm) | 408.66 | 262.40 | 0.20 |
| H-CP ($d$ = 0.4 mm) | 434.39 | 272.15 | 0.20 |
| Pristine CP | 456.97 | 296.60 | 0.20 |
| Heat treated CF | 149.50 | 85.74 | 0.61 |

the CF were arranged in the thickness direction despite the low fiber volume fraction.

Fig. 5 shows the CV curves with respect to the hole size. The two dominant peaks corresponding to $VO^{2+}/VO_2{}^+$ redox reactions appeared in the CV curves for the H-CP electrodes. As listed in Table 3, the current peaks at the anode ($I_{pa}$) and the cathode ($I_{pc}$) increased with a smaller hole size, indicating an increase in the reactivity. The increase in reactivity was closely related to the electrical conductivity and reaction sites. Therefore, the smaller laser cut volume had relatively large reaction sites and high electrical conductivity, demonstrating high electrochemical dynamics in the vanadium redox reaction. While laser processing 1–3% of the area, the effect of change in electrochemical properties due to the effect of heat treatment is insignificant compared to the pristine CP electrodes. Additionally, the reversibility of the redox reaction was evaluated using the difference between the anodic and cathodic peak potentials, called "current peak potential separation" ($\Delta E = E_{pa} - E_{pc}$). From the results of the current peak potential separation ($\Delta E$), shown in Table 3, it was confirmed that the reversible performance of the CP electrode did not change, although the apparent reaction volume of the electrode was reduced to make the patterns. In addition, compared to CF electrodes, the ASR of CP electrodes is relatively low, but it can be confirmed that CP electrodes have a greater reactivity due to the large reaction sites.

### 3.3. Numerical analysis results

Fig. 6 shows schematic models of the three electrodes for the numerical flow simulations and cross-sections (A–B) perpendicular to the electrolyte flow direction. The models were partitioned to check the flow rate at each electrode location. The pristine CP electrode consisted of the CP part and its side space between the flow frame and electrode. The H-CP electrode can be divided into three parts in the flow direction: Part 1, where the electrolyte flows along the holes; Part 2, which is the rest of the CP; and the side, as shown in Fig. 6(b). In the case of the V-CP electrode, Part 1′ comprises the overall volume of channels induced by the patterning process, Part 2′ is the rest of the CP, and the space between the CP and flow frame is the side, as shown in Fig. 6(c).

The electrolyte flow through the CP can be defined as reactive flow, which is highly involved in a redox reaction while passing through the CP. The flow through Part 1 can also be defined as a reactive flow because the flow through the discontinuous holes in Part 1 must pass through the CP. The electrolyte flow through Part 1′ of the V-CP electrode was defined as the dummy flow because it was less involved in the redox reaction while passing through the channel. The flow through the side where the electrolyte flows along the outer edge of the CP is also defined as a dummy flow because most of it flowing around the CP did not participate in the redox reaction without any significant flow resistance.

Table 4 shows the flow analysis results with respect to the electrodes. The average flow rate of the side space decreased and the reactive flow rate increased in the H-CP electrodes compared with the pristine CP electrodes because the holey pattern increased the overall porosity of the electrode. This tendency was more pronounced as the hole size increased. It is interesting to note that Part 1 had a relatively small volume compared with Part 2, but it had a relatively large flow rate per unit area. This means that, although there was no real flow channel, the holey pattern acted similarly to the flow channel along the hole. The flow phenomenon that had the same effect as the flow channel along the holes was named the "pseudo-channel effect." It should be noted that the reduced side flow of the H-CP electrode shown in Table 4 was redistributed through the CP owing to the pseudo-channel effect.

In the case of the V-CP, the flow rate in the electrode increased because the side flow rate was substantially reduced compared with that of the pristine CP. However, most of the flow rate through the channel (Part 1'), except for the flow along the channel

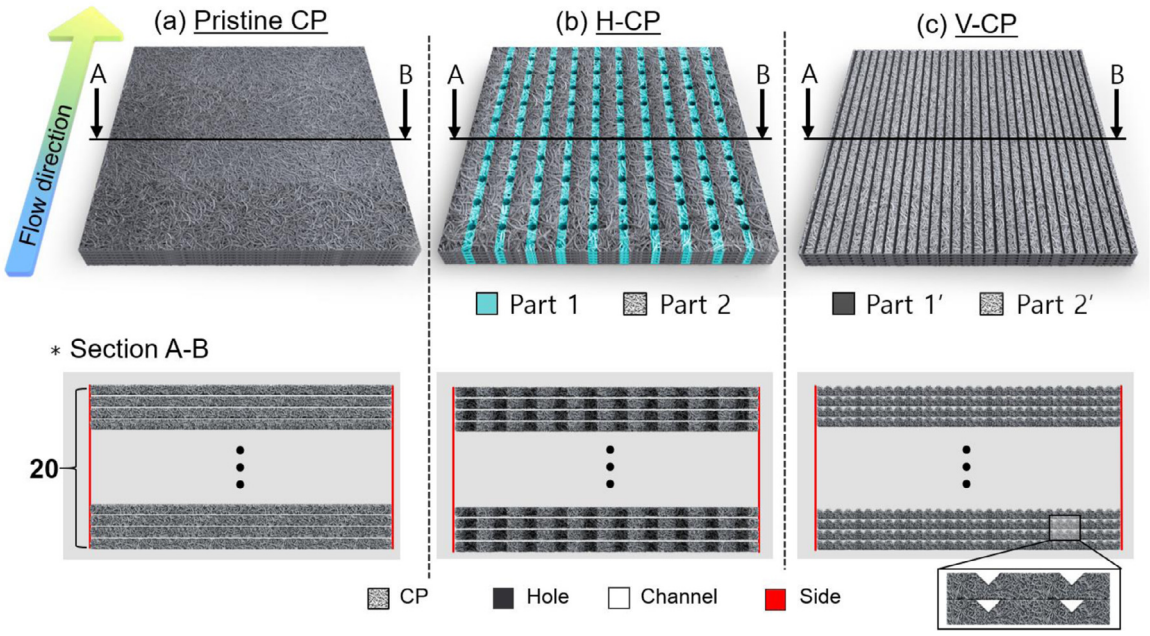


**Fig. 6.** Schematic models of the CP electrodes for the numerical flow simulations; (a) Pristine CP, (b) H-CP, (c) V-CP.

**Table 4**
Flow analysis results with respect to the electrodes.

| | Volume ratio | Average flow rate ($10^{-4}$ kg/s) | | | Flow rate per unit area ($10^{-4}$ kg/mm$^2$s) | |
|---|---|---|---|---|---|---|
| | (Part 1/Part 2) | Part 1(Part 1') | Part 2(Part 2') | Side | Part 1 | Part 2 |
| **H-CP ($d$ = 0.6mm)** | 0.25 | 5.20(29%) | 9.51(53%) | 3.20(18%) | 0.29 | 0.13 |
| **H-CP ($d$ = 0.5mm)** | 0.20 | 4.34(24%) | 10.36(58%) | 3.21(18%) | 0.29 | 0.14 |
| **H-CP ($d$ = 0.4mm)** | 0.15 | 3.47(19%) | 11.20(63%) | 3.24(18%) | 0.29 | 0.14 |
| **V-CP** | 0.02 | 9.68(54%) | 6.66(37%) | 1.57(9%) | 3.81 | 0.08 |
| **Pristine CP** | 0 | - | 13.89(78%) | 4.02(22%) | - | 0.15 (% of total flow rate) |

surface, was the dummy flow, which could not react with the CP. In addition, it should be noted that although the side flows of the H-CP electrodes were slightly larger than those of the V-CP electrode, the reactive flow of the H-CP electrodes (Parts 1 and 2) were larger than those of the V-CP electrode (Part 2′).

To analyze the mechanism of the pseudo-channel effect, the flow characteristics of the electrolyte were investigated in the vicinity of the holey pattern. Fig. 7(a) shows the pressure distribution around the holes. The pressure of the hole was lower than that of the adjacent CP in the flow direction. This is because the fluid requires higher pressure when passing through a porous structure than when passing through the hole. From the result, it can be concluded that the electrolyte flows from the tip to the tail of the hole following the direction of the arrow in Fig. 7(a). This was confirmed by the pressure gradient in the $y$-axis direction, as shown in Fig. 7(b). Based on the pressure gradient, the electrolyte converges at the hole tip and diverges at the tail. The pressure gradient in the $x$-axis direction, shown in Fig. 7(c), demonstrates that the dominant flow occurs along the holes, confirming the existence of the pseudo-channel effect.

### 3.4. VRFB single-cell test results

Fig. 8(a) shows the charge/discharge curve of the CP electrodes according to the hole size at 100 mA cm$^{-2}$. The H-CP electrode showed a lower charge/discharge overpotential and higher charge/discharge capacity than those of the pristine CP electrode. In the initial state of the charge/discharge process, the reduced overpotential was intimately associated with the enhanced distribution of the electrolyte and a substantial increase in the reactive surface area with the electrolyte in the electrode, even though the electrical resistance and the overall electrode volume were reduced compared with those of the pristine CP electrode. In particular, the H-CP ($d$ = 0.5 mm) electrode showed prolonged charge/discharge curves compared with the other H-CP electrodes, resulting from the tradeoff relationships between the electrochemical properties and the reactive surface areas [29]. In the case of the H-CP electrode with a larger hole size ($d$ = 0.6 mm), the reactive surface area increased owing to the increased pseudo-channel effect, reducing the activation overpotential. However, the H-CP electrode with a smaller hole size ($d$ = 0.4 mm), which had a higher electrical conductivity, showed a reduced ohmic overpotential. In addition, the H-CP ($d$ = 0.5 mm) electrode had a longer charge/discharge curve than the V-CP, resulting from a large reactive flow at the same electrical conductivity.

Fig. 8(b) shows the average coulombic efficiency (CE) and voltage efficiency (VE) of the VRFBs over 30 cycles. The CE, the ratio of charge/discharge capacity, quantitatively indicates irreversibility, such as vanadium ion permeation, side reaction, and electrode corrosion during the VRFB cell test [37–39]. For this reason, the CE is mainly affected by the electrode material, operation condition, and other VRFB cell parts. The results showed that the difference in CE between the electrodes was negligible because the same CP materials, operating conditions, and VRFB cell parts, such as membranes and bipolar plates, were used in the cell tests. The VE, the ratio of average discharge/charge voltage, quantitatively indicates low overpotential, such as activation loss, ohmic loss, and concentration loss, during the VRFB cell test [40]. The H-CP ($d$ = 0.5 mm)

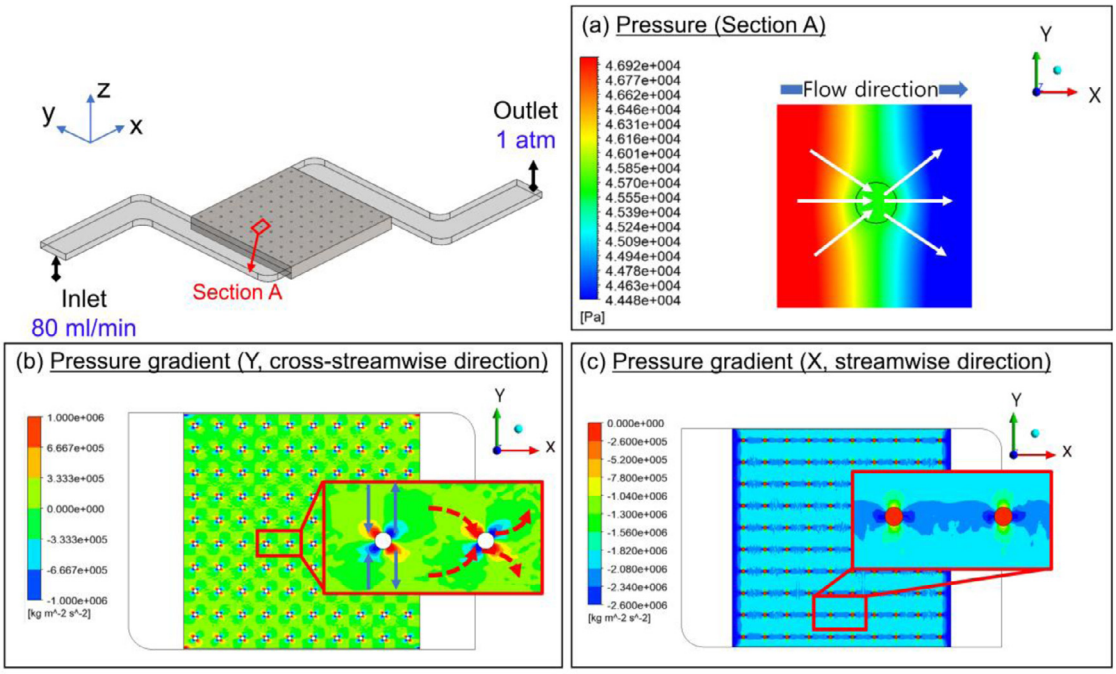


**Fig. 7.** Numerical simulation results; (a) pressure distribution around a hole, (b) pressure gradient along cross-streamwise direction, (c) pressure gradient along streamwise direction.

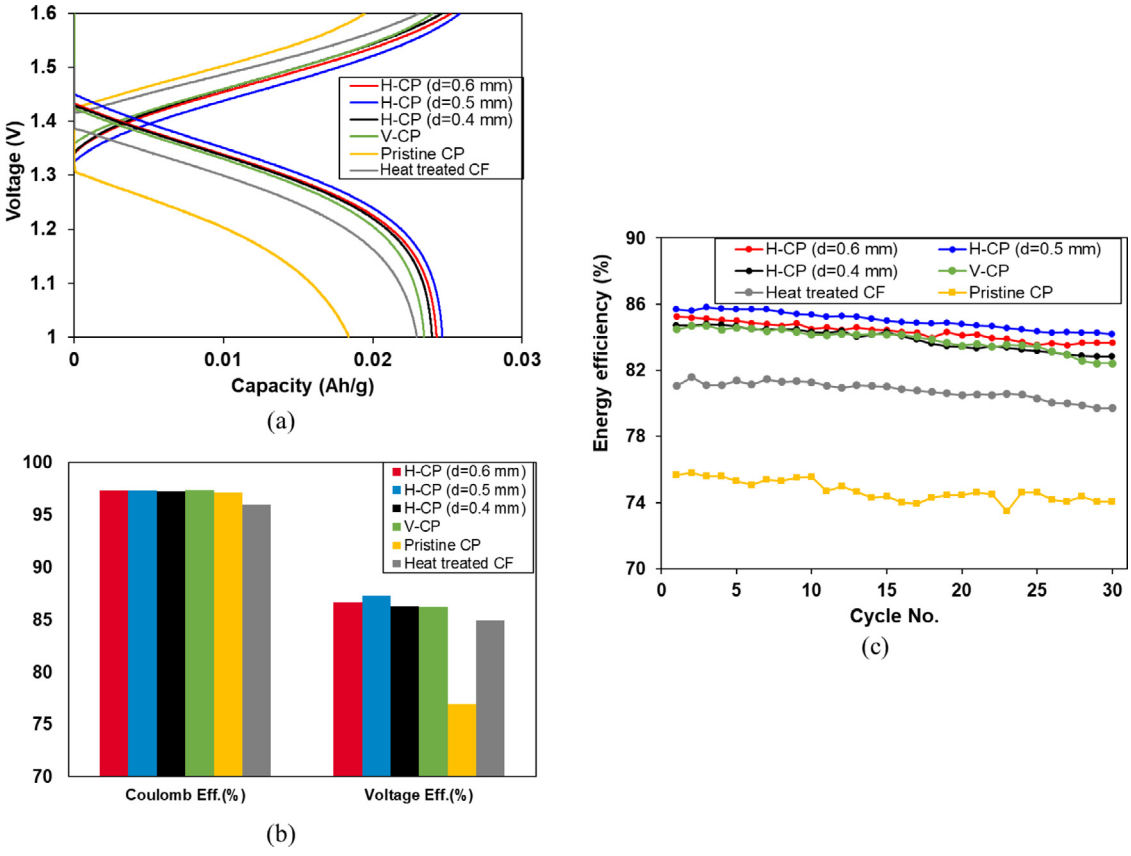


**Fig. 8.** VRFB single cell test results; (a) charge/discharge curve, (b) average CE, VE of the electrodes during 30 cycles, (c) EE of the electrodes.

**Table 5**
Energy efficiency with respect to the electrodes during 30 cycles.

| | H-CP ($d$ = 0.6 mm) | H-CP ($d$ = 0.5 mm) | H-CP ($d$ = 0.4 mm) | V- CP | Pristine CP | Heat-treated CF |
|---|---|---|---|---|---|---|
| Average efficiency (%) | 84.34 | 85.11 | 83.88 | 83.86 | 74.70 | 80.77 |

**Table 6**
The state of the art of carbon paper (CP) electrodes in VRFBs.

| Years | Current density [mA $cm^{-2}$] | Electrode-refinement | Energy efficiency [%] | | | Ref. |
|---|---|---|---|---|---|---|
| | | Surface treatment (S)/Pattern (P) | Pristine CP | Refined CP | Inc. | |
| | 100 | Pseudo-channel (P) | 74.70 | 85.11 | 10.41 | |
| 2020 | 100 | $SnO_2$ particle (S) | 72 | 78 | 6 | [41] |
| 2020 | 100 | $SnO_2$-Sb (S) | 72 | 78.7 | 6.7 | [42] |
| 2020 | 40 | Nitrogen-nanostructures (S) | 67 | 73 | 6 | [43] |
| 2019 | 100 | Nanopores (S) | - | 86 | - | [44] |
| 2019 | 100 | $MnO_2$ nanosheet array (S) | 60.4 | 66.4 | 6 | [45] |
| 2019 | 120 | Gradient porous (P) | 82.33 | 84.56 | 2.23 | [29] |
| 2018 | 50 | $SO_3H$-functionalized (S) | 75.7 | 80.8 | 5.1 | [46] |
| 2016 | 200 | KOH activation (S) | 73 | 88 | 15 | [47] |
| 2016 | 100 | TiC (S) | 68.4 | 80.7 | 12.3 | [48] |
| 2015 | 100 | Thermal activation (S) | 77 | 86 | 9 | [15] |

electrode showed the highest VE (87.37%) resulting from the lowest cell overpotential. As shown in Fig. 8(c), the EE results, the product of VE and CE, confirmed that the H-CP ($d$ = 0.5 mm) electrodes had the highest value among all the electrodes, and there was no substantial change in the slope of efficiency over 30 cycles. Table 5 summarizes the average EE of the electrodes over 30 cycles. The H-CP ($d$ = 0.5 mm) electrode has a low electrical conductivity but a high carbon fiber volume fraction, resulting in higher average EE (85.11%) of 4.34% than heat treated CF electrodes. When compared with the pristine CP electrode, the EE of the H-CP electrode increased by 10.41%, resulting from the low activation overpotential due to the large reactive surface area contacting the electrolyte. For a similar reason, the H-CP electrode showed higher average EE than the V-CP electrode, although the two electrodes had the same electrical resistance and reaction sites. From the results of the numerical analysis of the flow characteristics, one can infer that the difference in reactive surface area comes from the difference in the reactive flow rate, which is actually involved in the redox reaction. These results confirmed that the pseudo-channel effect of the H-CP improved the EE by substantially enhancing the overall flow characteristics inside the electrode.

Table 6 summarizes the state of the art of CP electrodes in VRFBs [15,29,41–48]. As shown in Table 6, the increase in efficiency of our study is superior to other studies measured under similar experimental conditions, and it is expected that there will be more improvement in the efficiency when additional surface treatments are applied to the H-CP.

## 4. Conclusion

In this study, to improve the EE of a VRFB, CPs were patterned and stacked to create an flow-through type electrode. The electrolyte flow characteristics with respect to the patterns were analyzed by means of numerical simulations, and the performance of the electrode was estimated through VRFB single-cell tests. The following results were obtained.

(1) The ASR of the patterned CPs increased, but the reversible performance of the patterned CPs was unchanged compared with the pristine CP, although the apparent reaction volume of the CPs was reduced to make the patterns.
(2) The average flow rate of the side space decreased and the reactive flow rate increased in the H-CPs compared with those of the pristine CP because the holey pattern increased the overall porosity of the electrode. This tendency was more pronounced as the hole size increased.
(3) The holey pattern acts similar to the flow channel along the holes, and this flow phenomenon, which has the same effect as the flow channel along holes, was named the “pseudo-channel effect.”
(4) The H-CP ($d$ = 0.5 mm) electrode showed the highest voltage efficiency (87.37%) because it had the lowest cell overpotential.
(5) The H-CP ($d$ = 0.5 mm) electrode had the maximum average EE (85.11%), which is 4.34% higher than that of the heat treated CF electrode, owing to the higher carbon fiber volume fraction.
(6) When compared with that of the pristine CP electrode, the EE of the H-CP electrode increased by 10.41%, resulting from the low activation overpotential caused by the large reactive surface area in contact with the electrolyte.

These results confirmed that CP with a pseudo-channel effect is a promising electrode for improving the EE of VRFBs by enhancing the flow characteristics of the electrolyte.

## Declaration of Competing Interest

The authors declare that they have no known competing financial interests or personal relationships that could have appeared to influence the work reported in this paper. The authors declare the following financial interests/personal relationships which may be considered as potential competing interests.

## CRediT authorship contribution statement

**Jae-Moon Jeong:** Conceptualization, Methodology, Software, Validation, Investigation, Writing – original draft. **Kwang Il Jeong:** Methodology, Investigation. **Jae Hyung Oh:** Methodology, Investigation. **Yong Sik Chung:** Resources, Investigation. **Seong Su Kim:** Conceptualization, Writing – review & editing, Supervision.

## Acknowledgments

This work was supported by the National Research Foundation of Korea (NRF) grant funded by the Korea government (MSIT) (No. 2020R1A2C2010965). This work was also financially supported by "Human Resources Program in Energy Technology" of the Korea Institute of Energy Technology Evaluation and Planning (KETEP), granted financial resource from the Ministry of Trade, Industry & Energy, Republic of Korea. (No. 20204030200050).

## Supplementary materials

Supplementary material associated with this article can be found, in the online version, at doi:10.1016/j.apmt.2021.101139.

## References

[1] L. Wei, X. Fan, H. Jiang, K. Liu, M. Wu, T. Zhao, Enhanced cycle life of vanadium redox flow battery via a capacity and energy efficiency recovery method, J. Power Sources 478 (2020) 228725.
[2] F. Jiang, W. Liao, T. Ayukawa, S.H. Yoon, K. Nakabayashi, J. Miyawaki, Enhanced performance and durability of composite bipolar plate with surface modification of cactus-like carbon nanofibers, J. Power Sources 482 (2021) 228903.
[3] A. Trovò, Battery management system for industrial-scale vanadium redox flow batteries: features and operation, J. Power Sources 465 (2020) 228229.
[4] Y. Jiang, G. Cheng, Y. Li, Z. He, J. Zhu, W. Meng, et al., Promoting vanadium redox flow battery performance by ultra-uniform ZrO2@ C from metal-organic framework, Chem. Eng. J. 415 (2021) 129014.
[5] Y. Jiang, M. Du, G. Cheng, P. Gao, T. Dong, J. Zhou, et al., Nanostructured N–doped carbon materials derived from expandable biomass with superior electrocatalytic performance towards V2+/V3+ redox reaction for vanadium redox flow battery, J. Energy Chem. 59 (2021) 706–714.
[6] W. Lee, M. Jung, D. Serhiichuk, C. Noh, G. Gupta, C. Harms, et al., Layered composite membranes based on porous PVDF coated with a thin, dense PBI layer for vanadium redox flow batteries, J. Membr. Sci. 591 (2019) 117333.
[7] B. Li, M. Gu, Z. Nie, Y. Shao, Q. Luo, X. Wei, et al., Bismuth nanoparticle decorating graphite felt as a high-performance electrode for an all-vanadium redox flow battery, Nano Lett. 13 (2013) 1330–1335.
[8] A. Ejigu, M. Edwards, DA. Walsh, Synergistic catalyst–support interactions in a graphene–$Mn_3O_4$ electrocatalyst for vanadium redox flow batteries, ACS Catal. 5 (2015) 7122–7130.
[9] Y. Gao, H. Wang, Q. Ma, A. Wu, W. Zhang, C. Zhang, et al., Carbon sheet-decorated graphite felt electrode with high catalytic activity for vanadium redox flow batteries, Carbon 148 (2019) 9–15.
[10] M. Jung, W. Lee, N.N. Krishnan, S. Kim, G. Gupta, L. Komsiyska, et al., Porous–nafion/PBI composite membranes and nafion/PBI blend membranes for vanadium redox flow batteries, Appl. Surf. Sci. 450 (2018) 301–311.
[11] B. Li, M. Gu, Z. Nie, X. Wei, C. Wang, V. Sprenkle, et al., Nanorod niobium oxide as powerful catalysts for an all vanadium redox flow battery, Nano Lett. 14 (2014) 158–165.
[12] W. Lee, C. Jo, S. Youk, H.Y. Shin, J. Lee, Y. Chung, et al., Mesoporous tungsten oxynitride as electrocatalyst for promoting redox reactions of vanadium redox couple and performance of vanadium redox flow battery, Appl. Surf. Sci. 429 (2018) 187–195.
[13] B. Sun, M. Skyllas-Kazacos, Modification of graphite electrode materials for vanadium redox flow battery application-I. Thermal treatment, Electrochim. Acta 37 (1992) 1253–1260.
[14] B. Sun, M. Skyllas-Kazacos, Chemical modification of graphite electrode materials for vanadium redox flow battery application—part II. Acid treatments, Electrochim. Acta 37 (1992) 2459–2465.
[15] A.M. Pezeshki, J.T. Clement, G.M. Veith, T.A. Zawodzinski, MM. Mench, High performance electrodes in vanadium redox flow batteries through oxygen-enriched thermal activation, J. Power Sources 294 (2015) 333–338.
[16] C. Flox, M. Skoumal, J. Rubio-Garcia, T. Andreu, JR. Morante, Strategies for enhancing electrochemical activity of carbon-based electrodes for all-vanadium redox flow batteries, Appl. Energy 109 (2013) 344–351.
[17] E. Bulska, W. Jędral, E. Kopyść, H. Ortner, S. Flege, Secondary ion mass spectrometry for characterizing antimony, arsenic and selenium on graphite surfaces modified with noble metals and used for hydride generation atomic absorption spectrometry, Spectrochim. Acta Part B 57 (2002) 2017–2029.
[18] W. Wang, X. Wang, Investigation of Ir-modified carbon felt as the positive electrode of an all-vanadium redox flow battery, Electrochim. Acta 52 (2007) 6755–6762.
[19] Z. González, A. Sánchez, C. Blanco, M. Granda, R. Menéndez, R. Santamaría, Enhanced performance of a Bi-modified graphite felt as the positive electrode of a vanadium redox flow battery, Electrochem. Commun. 13 (2011) 1379–1382.
[20] R. Wang, Y. Li, Carbon electrodes improving electrochemical activity and enhancing mass and charge transports in aqueous flow battery: Status and perspective, Energy Storage Mater. 31 (2020) 230–251.
[21] J. Sun, H. Jiang, C. Zhao, X. Fan, C. Chao, T. Zhao, Holey aligned electrodes through *in-situ* ZIF-8-assisted-etching for high-performance aqueous redox flow batteries, Sci. Bull. 66 (2021) 904–913.
[22] M. Kazacos, M. Skyllas-Kazacos, Performance characteristics of carbon plastic electrodes in the all-vanadium redox cell, J. Electrochem. Soc. 136 (1989) 2759.
[23] B. Sun, M. Skyllas-Kazakos, Chemical modification and electrochemical behavior of graphite fibre in acidic vanadium solution, Electrochim. Acta 36 (1991) 513–517.
[24] K.J. Kim, M.S. Park, Y.J. Kim, J.H. Kim, S.X. Dou, M. Skyllas-Kazacos, A technology review of electrodes and reaction mechanisms in vanadium redox flow batteries, J. Mater. Chem. A 3 (2015) 16913–16933.
[25] C. Dennison, E. Agar, B. Akuzum, E. Kumbur, Enhancing mass transport in redox flow batteries by tailoring flow field and electrode design, J. Electrochem. Soc. 163 (2016) A5163–A51A9.
[26] C. Dennison, E. Agar, B. Akuzum, E. Kumbur, Enhancing mass transport in redox flow batteries by tailoring flow field and electrode design, J. Electrochem. Soc. 163 (2015) A5163.
[27] D. Aaron, Q. Liu, Z. Tang, G. Grim, A. Papandrew, A. Turhan, et al., Dramatic performance gains in vanadium redox flow batteries through modified cell architecture, J. Power Sources 206 (2012) 450–453.
[28] I. Mayrhuber, C. Dennison, V. Kalra, E. Kumbur, Laser-perforated carbon paper electrodes for improved mass-transport in high power density vanadium redox flow batteries, J. Power Sources 260 (2014) 251–258.
[29] H. Jiang, B. Zhang, J. Sun, X. Fan, W. Shyy, T. Zhao, A gradient porous electrode with balanced transport properties and active surface areas for vanadium redox flow batteries, J. Power Sources 440 (2019) 227159.
[30] J. Houser, J. Clement, A. Pezeshki, MM. Mench, Influence of architecture and material properties on vanadium redox flow battery performance, J. Power Sources 302 (2016) 369–377.
[31] J. Houser, A. Pezeshki, J.T. Clement, D. Aaron, MM. Mench, Architecture for improved mass transport and system performance in redox flow batteries, J. Power Sources 351 (2017) 96–105.
[32] M. Al-Yasiri, J. Park, Study on channel geometry of all-vanadium redox flow batteries, J. Electrochem. Soc. 164 (2017) A1970.
[33] D. Maggiolo, F. Zanini, F. Picano, A. Trovo, S. Carmignato, M. Guarnieri, Particle based method and X-ray computed tomography for pore-scale flow characterization in VRFB electrodes, Energy Storage Mater. 16 (2019) 91–96.
[34] Q. Xu, T. Zhao, C. Zhang, Performance of a vanadium redox flow battery with and without flow fields, Electrochim. Acta 142 (2014) 61–67.
[35] J. Lee, J. Kim, H. Park, Numerical simulation of the power-based efficiency in vanadium redox flow battery with different serpentine channel size, Int. J. Hydrog. Energy 44 (2019) 29483–29492.
[36] X. Ma, H. Zhang, F. Xing, A three-dimensional model for negative half cell of the vanadium redox flow battery, Electrochim. Acta 58 (2011) 238–246.
[37] W. Liao, Y. Zhang, X. Zhou, M. Zhuang, D. Guo, F. Jiang, et al., Low-carbon-content composite bipolar plates: a novel design and its performance in vanadium redox flow batteries, ChemistrySelect 4 (2019) 2421–2427.
[38] C. Zhang, T. Zhao, Q. Xu, L. An, G. Zhao, Effects of operating temperature on the performance of vanadium redox flow batteries, Appl. Energy 155 (2015) 349–353.
[39] Q. Xu, Y. Ji, L. Qin, P. Leung, F. Qiao, Y. Li, et al., Evaluation of redox flow batteries goes beyond round-trip efficiency: a technical review, J. Energy Storage 16 (2018) 108–115.
[40] L. Wei, H. Jiang, Y. Ren, M. Wu, J. Xu, T. Zhao, Investigation of an aqueous rechargeable battery consisting of manganese tin redox chemistries for energy storage, J. Power Sources 437 (2019) 226918.
[41] X. He, Z. He, Q. Zou, L. Wu, Carbon paper decorated with tin dioxide particle via *in situ* electrodeposition as bifunctional electrode for vanadium redox flow battery, Int. J. Energy Res. 44 (2020) 2100–2109.
[42] R. Zhang, K. Li, S. Ren, J. Chen, X. Feng, Y. Jiang, et al., Sb-doped SnO2 nanoparticle-modified carbon paper as a superior electrode for a vanadium redox flow battery, Appl. Surf. Sci. (2020) 146685.
[43] A. Sodiq, F. Fasmin, L. Mohapatra, S. Mariyam, M. Arunachalam, H. Hamoudi, et al., Enhanced electrochemical performance of modified thin carbon electrodes for all-vanadium redox flow batteries, Mater. Adv. 1 (2020) 2033–2042.
[44] S. Abbas, S. Mehboob, H.J. Shin, O.H. Han, HY. Ha, Highly functionalized nanoporous thin carbon paper electrodes for high energy density of zero-gap vanadium redox flow battery, Chem. Eng. J. 378 (2019) 122190.
[45] Y. Jiang, X. Feng, G. Cheng, Y. Li, C. Li, Z. He, et al., Electrocatalytic activity of $MnO_2$ nanosheet array-decorated carbon paper as superior negative electrode for vanadium redox flow batteries, Electrochim. Acta 322 (2019) 134754.
[46] Z. He, Y. Jiang, Y. Li, J. Zhu, H. Zhou, W. Meng, et al., Carbon layer-exfoliated, wettability-enhanced, $SO_3H$-functionalized carbon paper: a superior positive electrode for vanadium redox flow battery, Carbon 127 (2018) 297–304.
[47] X. Zhou, Y. Zeng, X. Zhu, L. Wei, T. Zhao, A high-performance dual-scale porous electrode for vanadium redox flow batteries, J. Power Sources 325 (2016) 329–336.
[48] L. Wei, T. Zhao, L. Zeng, X. Zhou, Y. Zeng, Titanium carbide nanoparticle-decorated electrode enables significant enhancement in performance of all-vanadium redox flow batteries, Energy Technol. 4 (2016) 990–996.